Mass Spectrometry On-Line Monitoring and MS^2 Product Characterization of TiO_2/UV Photocatalytic Degradation of Chlorinated Volatile Organic Compounds

Rosana M. Alberici, Maria Anita Mendes, Wilson F. Jardim, and Marcos N. Eberlin

State University of Campinas, UNICAMP Institute of Chemistry, Campinas, SP Brazil

On-line Mass Spectrometry and MS^2 are applied to monitor and identify the by-products and total mineralization products of TiO_2/UV photocatalytic degradation of four chlorinated volatile organic compounds (VOCs): trichloroethylene (TCE), tetrachloroethylene (TeCE), chloroform, and dichloromethane. Selected multiple ion mass spectrometry monitoring using characteristic 70 eV electron ionization ionic fragments monitors in real time the destruction of the starting VOC and the formation of by-products, i.e., the degrees of VOC mineralization, as a function of the flow and relative humidity of the carrier gas (synthetic air). Several by-products were detected: phosgene for TCE, TeCE, and chloroform; dichloroacetyl chloride for TCE; and trichloroacetyl chloride for TeCE. Cl_2 and CO_2 were also detected as final mineralization products of the four chlorinated VOCs. Structural characterization of by-products was accomplished via MS^2 collision-induced dissociation of molecular ions or characteristic ionic fragments. (J Am Soc Mass Spectrom 1998, 9, 1321–1327) © 1998 American Society for Mass Spectrometry

Chlorinated volatile organic compounds (VOC) are widely used as industrial solvents, particularly for degreasing of metals and for dry cleaning; hence, they are common contaminants in gaseous emissions from industrial processes, landfills, hazardous waste sites, groundwater remediation facilities, and indoor air [1]. Because many chlorinated VOCs are carcinogenic or toxic, or both, concern has been increasing about the control and reduction of their concentration in the atmosphere, which has created an urgent demand for effective and inexpensive techniques for the destruction of chlorinated VOCs.

Heterogeneous TiO_2 photocatalysis, a potential method for the destruction of many organic pollutants [2, 3], mineralizes efficiently several classes of organic compounds in aqueous [4, 5] or gas-phase systems [6–12]. Dibble and Raupp [6, 7], for instance, reported complete gas-phase mineralization of TCE to CO_2 and HCl in a fluidized-bed TiO_2 photoreactor. Yamazaki-Nishida et al. [8] also reported gas-phase TCE photodegradation to CO_2 and HCl in a packed-bed reactor containing highly porous TiO_2 pallets. Nimlos et al. [9, 10], monitoring TCE photodegradation by molecular beam mass spectrometry (MBMS) and gas-phase Fourier transform infrared (FTIR), detected Cl_2, HCl, CO, and CO_2 but also two hazardous by-products: phosgene (Cl_2CO) and dichloroacetyl chloride [$Cl_2HCC(O)Cl$, DCAC]. Latter, Kutsuna et al. [11] observed that relative humidity, light intensity, and the organic compounds and O_2 concentrations influence the decay and degradation-product formation rates in TCE and TeCE photodegradation. We used an annular TiO_2-coated photoreactor illuminated by a 30 W UV source [12] for TCE photodegradation; GC-FID or GC-MS detected no by-products under the applied experimental conditions. These different experimental results under variable TiO_2/UV photocatalytic degradation conditions may result from the specific characteristics of each analytical tool used for monitoring. Therefore, for the practical use of this technology it is desirable to perform continuous, on-line monitoring of the TiO_2/UV photodegradation process using fast and reliable analytical tools. The on-line monitoring would help to set the best operating conditions not only for the destruction of the chlorinated VOCs, but also for complete mineralization with the total degradation of undesirable or even more hazardous by-products such as phosgene and DCAC.

We report here the use of a multiquadrupole mass spectrometer to monitor in real-time the gas-phase heterogeneous UV photodegradation of chlorinated VOCs in a TiO_2-catalyst flow reactor. Chlorinated VOC decay rates and by-product and final product formation

Address reprint requests to Dr. Marcos N. Eberlin, State University of Campinas, UNICAMP Institute of Chemistry, CP6154, 13083-970 Campinas, SP Brazil. E-mail: eberlin@iqm.unicamp.br

1044-0305/98/$19.00
PII S1044-0305(98)00112-3

Received March 12, 1998
Revised August 13, 1998
Accepted August 13, 1998

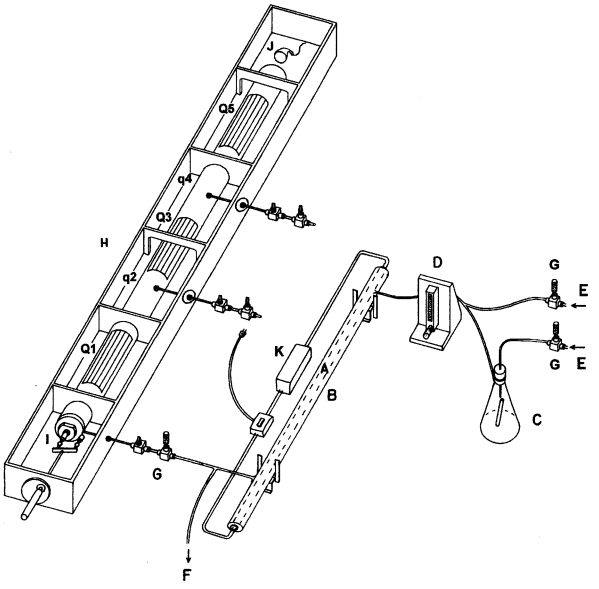

Figure 1. Schematic representation of the MS/MS^2 on-line monitoring photocatalytic degradation system. A—UV-visible lamp, B—photoreactor, C—VOC reservoir, D—flow meter, E—carrier gas, F—exit line, G—needle valve flow control, H—mass spectrometer, I—ion source, J—detector, K—light starter, Qn—quadrupole analysers, qn—collision cells. Items are not shown to scale.

rates were measured by selective multiple ion mass spectrometry monitoring (SIM-MS), whereas structural characterization was performed via MS^2 experiments on characteristic molecular or fragment ions.

Experimental

Powdered TiO_2 with a primary particle diameter of 30 nm, a crystal structure of primarily anatase, and a surface area of $50 \pm 15\ m^2\ g^{-1}$ (BET) was obtained from Degussa (P-25), and used as received. High-performance liquid chromatography (HPLC) grade chlorinated organic compounds were used to generated the contaminated atmosphere that continuously fed the photodegradation reactor.

The experimental setup for the photodegradation experiments (Figure 1) uses an annular photoreactor constructed with a glass cylinder (35 mm i.d. $\times$ 86 cm height) and a commercially available UV-visible source (30-W lamp from Sankyo Denki, Japan BLB) with maximum light intensity output at 365 nm and light flux of 7.56×10^{-9} einsteins $cm^{-2}\ s^{-1}$. The lamp (90 cm long, external diameter = 29 mm) serves as the inner surface of the annulus. The relatively small 400 mL internal volume results in short residence times for the continuous gaseous flux. A pentaquadrupole (QqQqQ) mass spectrometer [13] [Extrel (Pittsburgh, PA)] was used as the detecting system (Figure 1).

The glass tube internal wall was coated with TiO_2 using the simple soaking/drying coating method [12]. Because water and oxygen are required to maintain long-term catalyst photoactivity [14–17], commercially available (Air Liquid) synthetic air containing 20% O_2 and 80% N_2 with 20% or 80% relative humidity was used as the carrier gas. A more detailed description of the photocatalytic degradation experimental apparatus has been published elsewhere [12]. A small fraction of the reactor off-gases was fed continuously to the ion source of the mass spectrometer through a gas-inlet system (G in Figure 1). The chlorinated VOC concentration in the sample (C_{inlet}) was maintained at 500 ppmv by adjusting the flows into the mixing T (D in Figure 1) of both the VOC-doped synthetic air (C in Figure 1) and the VOC-free synthetic air. The doped synthetic air contained the VOC near its room-temperature (25 °C) vapor pressure. A standard 500 ppmv VOC synthetic air mixture was prepared and used for calibration.

In a typical experiment, a fraction of the gaseous mixture passing continuously through the atmospheric pressure TiO_2-coated photoreactor was sampled for mass spectrometric analysis. A blank mass spectrum was recorded, and sample mass spectra were background subtracted. The mixture was ionized by 70 eV electron ionization (EI), and multiple SIM was performed to follow destruction of the chlorinated VOCs and the formation of by-products and final products. SIM-MS monitoring uses the following ions (Table 1): m/z 95 for TCE, m/z 63 for phosgene, m/z 83 for DCAC, m/z 44 for carbon dioxide, m/z 166 for TeCE, m/z 117 for TCAC, m/z 83 for chloroform, and m/z 49 for dichloromethane.

Table 1. Major ions in the 70 eV EI mass spectra of selected compounds

Compound	Name	*m/z* (relative abundance)
$CHClCCl_2$	Trichloroethylene (TCE)	60(50), 62(16), 95(100), 97(64), 99(8), 130(90), 132(86), 134(28), 136(4)
CCl_2CCl_2	Tetrachloroethylene (TeCE)	82(5), 84(2), 94(37), 96(25), 98(2), 129(90), 131(75), 133(20), 164(90), 166(100), 168(45), 170(10)
$CHCl_3$	Chloroform	47(34), 48(16), 49(12), 50(4), 83(100), 85(62), 87(8)
CH_2Cl_2	Dichloromethane	47(14), 48(10), 49(100), 50(4), 51(24), 84(60), 86(34), 88(4)
$COCl_2$	Phosgene	63(100), 65(32), 98(8), 100(6), 102(2)
$CHCl_2C(O)Cl$	Dichloroacethyl chloride (DCAC)	63(38), 65(12), 76(11), 78(4), 83(100), 85(65), 87(10), 111(13), 113(8), 115(1), 146(8), 148(7), 150(1)
$CCl_3C(O)Cl$	Trichloroacetyl chloride (TCAC)	63(38), 65(12), 117(100), 119(96), 121(30), 145(2), 147(2), 149(1)
Cl_2	Molecular chlorine	70(100), 72(61), 74(8)
CO_2	Carbon dioxide	44(100)

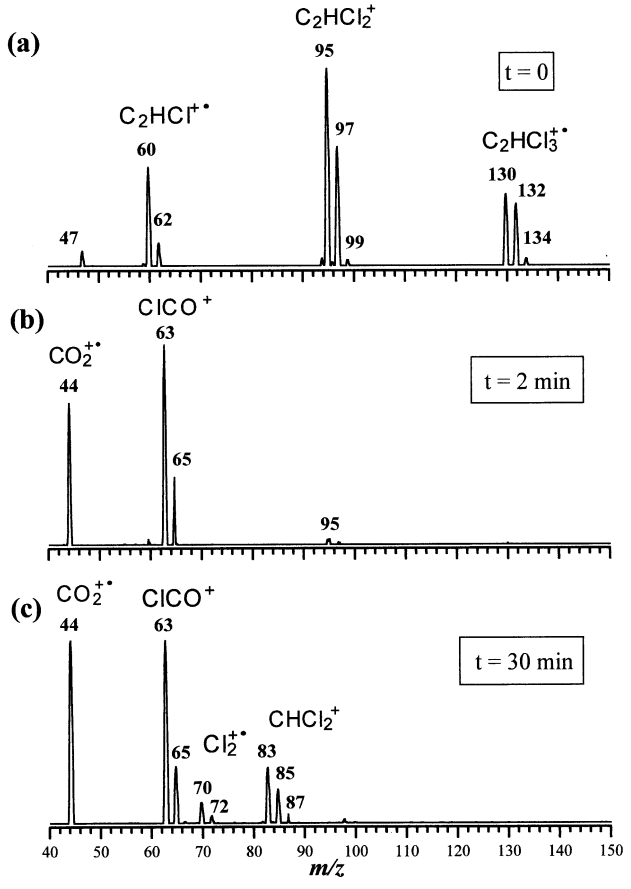

Figure 2. Mass spectra of the off-gas mixture sampled in various stages of TCE photocatalytic degradation: (**a**) $t = 0$, no irradiation, (**b**) $t = 2$ min, and (**c**) $t = 30$ min of UV irradiation. Experiments were performed with 20% relative humidity and a flow (Q) of 1000 mL min^{-1}.

For the MS^2 collision-induced dissociation (CID) experiments, an ion of interest was mass selected by the first quadrupole (Q1), and then subjected to 15 eV collisions with argon in q2. The CID fragments were analyzed by scanning Q5, while operating Q3 in the nonanalyzing rf-only mode. A PC-base data system [13a] was used to control the mass spectrometry and MS^2 scans.

Results and Discussion

Photocatalytic Degradation of TCE

Product identification. Figure 2 compares the 70 eV EI mass spectra obtained at various stages of TCE photocatalytic degradation. With no irradiation, the mass spectrum (Figure 2a) of the 500 ppmv TCE synthetic air mixture shows only the characteristic TCE fragment ions (Table 1). The UV light is turned on, and after 2 min the off-gas mass spectrum (Figure 2b) shows a sharp decrease in the abundance of the TCE fragment ions, which suggests nearly complete TCE destruction. CO_2 and phosgene are detected in the off-gas mixture by their characteristic fragment ions (Table 1) of m/z 44 ($CO_2^{+\cdot}$) and m/z 63/65 ($CO^{35}Cl^+$ and $CO^{37}Cl^+$). After 30 min of UV irradiation (Figure 2c), the system reaches a steady state in which DCAC and Cl_2 also participates; they are detected by their characteristic fragments of m/z 83/85 ($CHCl_2^+$) and m/z 70/72 ($Cl_2^{+\cdot}$).

These results suggest therefore that under the present TiO_2-photocatalytic degradation conditions, TCE is mineralized to CO_2 with Cl_2, phosgene, and DCAC participating as by-products. CO as a by-product and HCl as a final mineralization product have also been detected in other TCE degradation experiments [9, 10]. $CO^{+\cdot}$ of m/z 28 is isobaric with $N_2^{+\cdot}$; hence CO formation could not be monitored owing to the presence of N_2 in the carrier gas, and the unit mass resolution of the quadrupole mass analyzer. CO monitoring in the presence of N_2 can, however, be accomplished in quadrupole analyzers via the m/z 14/16 ratio, but this normally requires background-free spectra and calibration procedures with standard CO/N_2 mixtures. Failure to detect HCl likely results from its adsorption on the TiO_2 surface.

MS^2 experiments. Figure 3 shows the CID product spectra for the ions used to detect and monitor phosgene and DCAC. The DCAC closed-shell ion $CH^{35}Cl_2^+$ of m/z 83 loses, as expected, a neutral molecule of $H^{35}Cl$ to form $C^{35}Cl^+$ of m/z 47 (Figure 3a). Furthermore, $CH^{35}Cl^{37}Cl^+$ of m/z 85 (Figure 3b), as expected from its isotopically mixed composition, loses both $H^{35}Cl$ and $H^{37}Cl$ to produce $C^{37}Cl^+$ of m/z 49 and $C^{35}Cl^+$ of m/z 47. CO loss from the phosgene ions $CO^{35}Cl^+$ of m/z 63 (Figure 3c) and $CO^{37}Cl^+$ of m/z 65 (Figure 3d) produce $^{35}Cl^+$ (m/z 35) and $^{37}Cl^+$ (m/z 37), respectively. CO loss is a CID behavior characteristic of acylium ions [18].

Mass spectrometry on-line monitoring. Carrier gas flow and humidity effects. Figure 4 shows diagrams of the multiple SIM-MS on-line monitoring of TCE photocatalytic degradation performed at different carrier gas (synthetic air) flows. As the UV light is turned on, TCE is quickly destroyed. Phosgene and CO_2 are detected for all flows tested, but DCAC (an intermediate to phosgene production) is only detected at shorter TCE residence times, i.e., higher flows (1000 mL min^{-1} in Figure 4c). At higher flows, TCE degradation and phosgene production also take longer photodegradation times to stabilize. These findings show, therefore, that phosgene and DCAC formation can be controlled as a function of carrier gas flow, that is, of the TCE residence time in the TiO_2/UV photoreactor.

Figure 5 shows the off-gas mass spectrum in the steady state (after 30 min of irradiation) of TCE photocatalytic degradation at 80% relative humidity. It is clear that higher relative humidities decreases the efficiency of TCE destruction. The nearly complete TCE consumption at 20% relative humidity (Figure 2c) drops to 70% at relative humidity of 80% (Figure 5). Note in Figure 5 the characteristic TCE ions of m/z 95/97 and

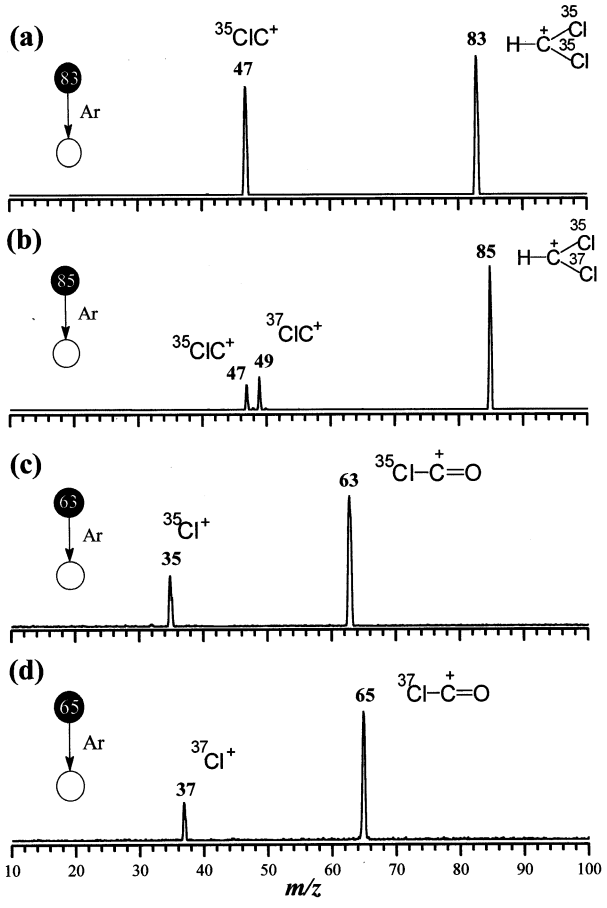

Figure 3. Double stage CID product ion spectra for selected ions used to monitor by-products in TCE photocatalytic degradation.

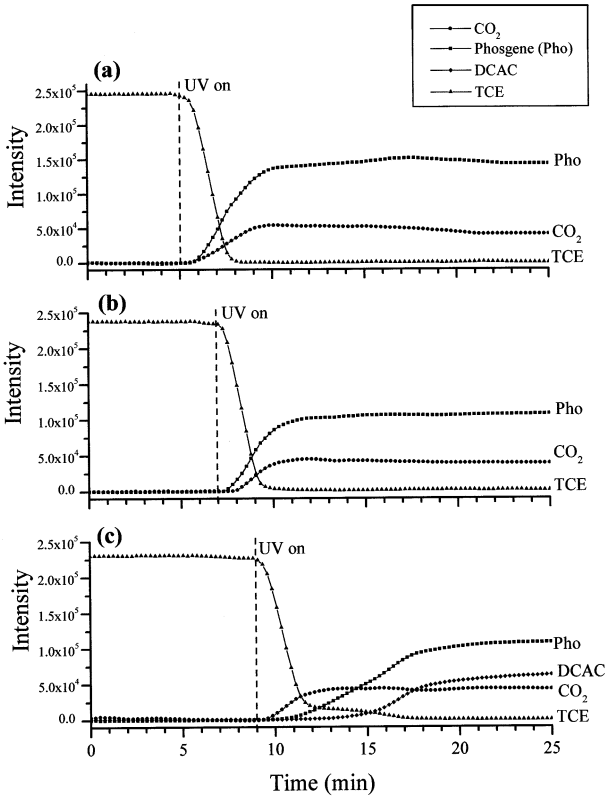

Figure 4. Diagrams of SIM-MS monitoring of TCE photocatalytic degradation performed with 20% relative humidity and variable flows: (**a**) Q = 100 mL min^{-1}, (**b**) Q = 500 mL min^{-1}, and (**c**) Q = 1000 mL min^{-1}.

130/132 and the absence of the DCAC ions of m/z 83/85. The retardation of the TiO_2/UV photocatalytic degradation process by higher relative humidities results probably from competitive adsorption of water vapor on the TiO_2 surface [11].

TiO_2/UV photocatalytic degradation mechanism of TCE. Nimlos et al. [9] proposed the mechanism depicted in Scheme **1** for TCE photocatalytic degradation in humidified air. Initially and under irradiation, water molecules adsorbed onto the TiO_2 surface form hydroxyl radicals ($OH^{\cdot}$), which attack TCE molecules to form chlorine atoms, which in turn add to TCE molecules at the CH carbon atom. The resulting radicals react with O_2 to form alkoxy radicals that either lose $Cl^{\cdot}$ to form DCAC or undergo C–C bond cleavage to form both phosgene and $Cl_2CH^{\cdot}$. The branching ratio for the two competing processes (a) and (b), see Scheme **1**, depends upon the relative strengths of the C–C and the C–Cl bonds of the alkoxy carbon. The DCAC by-product eventually forms phosgene by $Cl^{\cdot}$ attack via the reverse reaction (a). TCE degradation is completed by phosgene decomposition to CO, CO_2, Cl_2, and HCl. This mechanism has been substantiated by several pieces of experimental evidence [10, 19, 20]. For instance, chlorinated hydrocarbons are degraded much more efficiently than hydrocarbons [19], whereas the presence of TCE (a source of chlorine atoms) dramatically accelerates photocatalytic degradation of isooctane and toluene [20].

In Scheme **1**, the intermediates and final products identified in the present study, i.e., DCAC, phosgene, CO_2 and Cl_2, are highlighted in boxes. As depicted by pathway (a), the detection of DCAC only at higher carrier gas flows (Figure 4c), i.e., short TCE residence

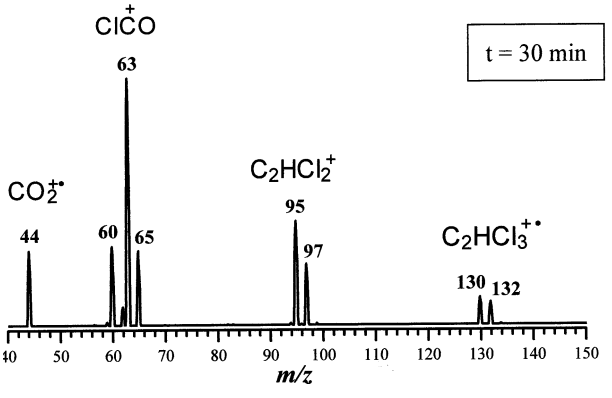

Figure 5. Mass spectrum of the off-gas mixture sampled in TCE photocatalytic degradation after 30 min of UV irradiation (steady state). Experiments were performed with Q = 1000 mL min^{-1} and relative humidity of 80%.

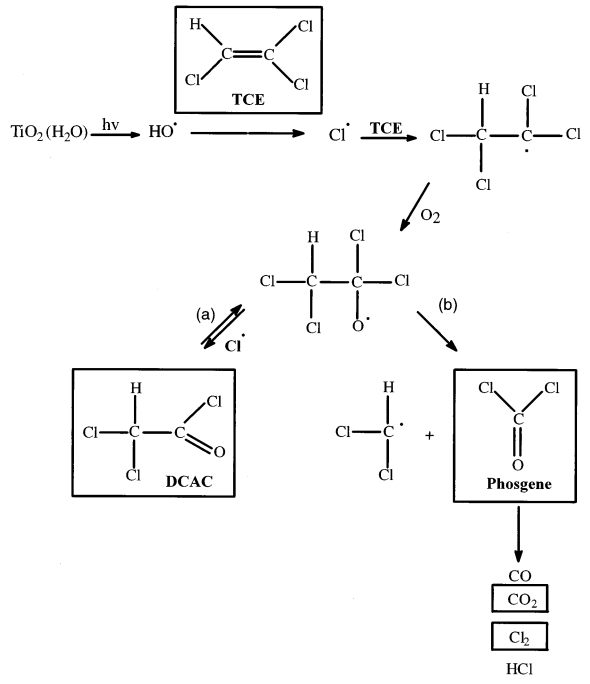

Scheme 1

times, agrees with its participation as a by-product to phosgene formation.

TeCE Photocatalytic Degradation

Product identification. Figure 6 compares the 70 eV EI mass spectra of the off-gas mixture sampled at various stages of TeCE photocatalytic degradation. With no irradiation, the spectrum (Figure 6a) shows only the characteristic fragment ions of TeCE (Table 1). After 2 min of irradiation (Figure 6b), partial degradation of TeCE occurs, and phosgene (m/z 63/65), Cl_2 (m/z 70/72/74), trichloroacetyl chloride [TCAC (m/z 117/119)], and CO_2 (m/z 44) are detected. No TeCE is detected after 10 min of irradiation; a steady state is reached and the characteristic ions of phosgene, TCAC and CO_2 dominate the mass spectrum (Figure 6c). Nimlos and co-workers [9] detected, in addition to CO and HCl, these same by-products of TeCE photocatalytic degradation.

Double stage (MS^2) CID experiments confirm TCAC formation (Figure 7). $^{35}Cl_3C^+$ of m/z 117 loses $^{35}Cl^{\cdot}$ to yield exclusively $C^{35}Cl_2^{+\cdot}$ of m/z 82 (Figure 7a). The isotopically mixed $C^{35}Cl_2^{37}Cl^+$ ion of m/z 119 loses either $^{35}Cl^{\cdot}$ or $^{37}Cl^{\cdot}$ to form the two fragments $^{35}Cl^{37}ClC^{+\cdot}$ (m/z 84) and $^{35}Cl_2C^{+\cdot}$ (m/z 82) in a 2:1 ratio, which reflects accurately the $^{35}Cl/^{37}Cl$ composition of the precursor ion.

According to Yamazaki-Nishida and co-workers [21], the TeCE photocatalytic degradation pathways are similar to those of TCE (Scheme **1**) except that, for TeCE, pathway (a) involves the three-chlorinated TCAC by-product.

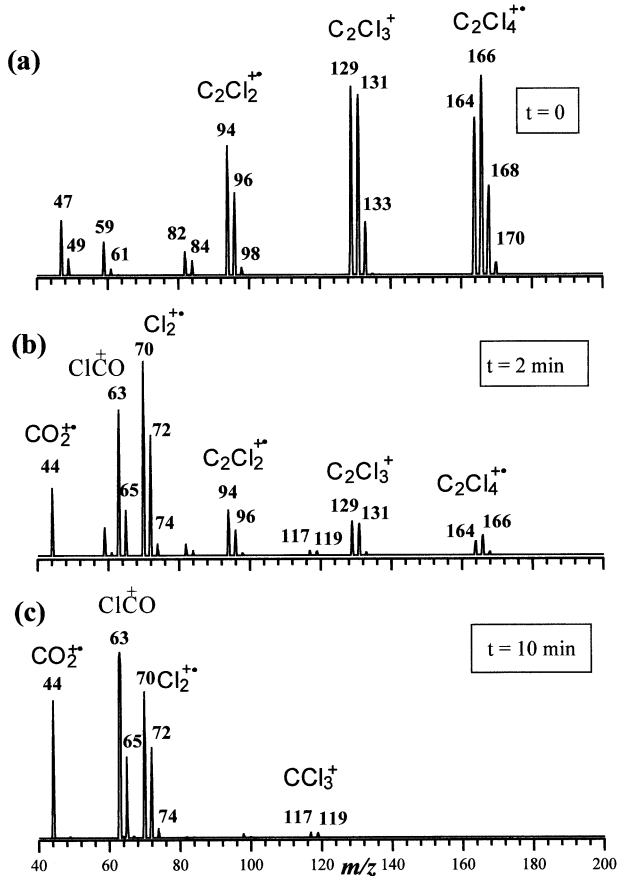

Figure 6. Mass spectra of the off-gas mixture sampled in various stages of TeCE photocatalytic degradation: (**a**) $t = 0$, no irradiation, (**b**) $t = 2$ min, and (**c**) $t = 10$ min of UV irradiation. Experiments were performed with 20% relative humidity and $Q = 500$ mL min^{-1}.

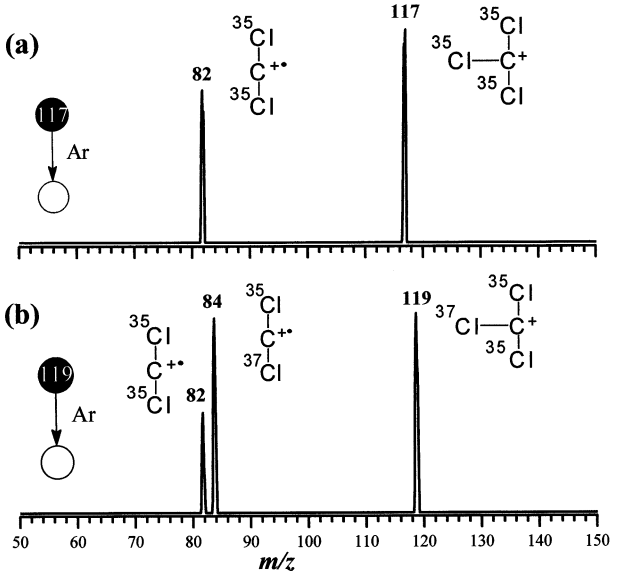

Figure 7. Double stage CID product ion spectra for selected ions used to monitor by-products in TeCE photocatalytic degradation.

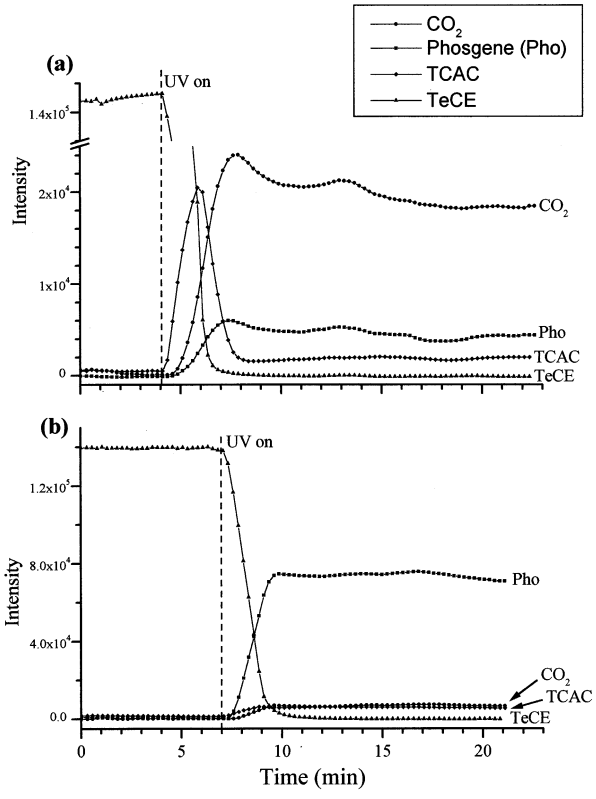

Figure 8. Diagrams of SIM-MS monitoring of TeCE photocatalytic degradation performed with 20% relative humidity and variable flows: (**a**) Q = 100 mL min^{-1} and (**b**) Q = 500 mL min^{-1}.

Mass spectrometry on-line monitoring: The effect of carrier gas flow. Figure 8 compares diagrams of multiple SIM-MS on-line monitoring of TeCE photocatalytic degradation performed at different carrier gas flows. At 100 mL min^{-1} (Figure 8a), TCAC is formed as a major product, but rapidly consumed in the first minutes of UV irradiation. When a steady state is reached, TCAC formation stabilizes in a low level. At 500 mL min^{-1} (Figure 8b), i.e., longer TeCE residence times in the photoreactor, relatively more phosgene and consequently less CO_2 are formed, whereas TCAC is detected at low, but constant, abundance.

Photocatalytic Degradation of $CHCl_3$ and CH_2Cl_2

Similar experiments were performed to monitor chloroform and dichloromethane photocatalytic degradation. The same by-products and final products were detected in the chloroform degradation experiments, i.e., phosgene, Cl_2 and CO_2. For dichloromethane, however, the m/z 63/65 ions ($ClCO^+$) observed in the mass spectrum of the off-gas mixture were attributed not to phosgene, but to formyl chloride. In dichloromethane photocatalytic degradation, formyl chloride is formed preferentially owing to its lower heat of formation when compared with that of phosgene [22]. An average of 50% degradation occur in both $CHCl_3$ and CH_2Cl_2 photocatalytic degradations.

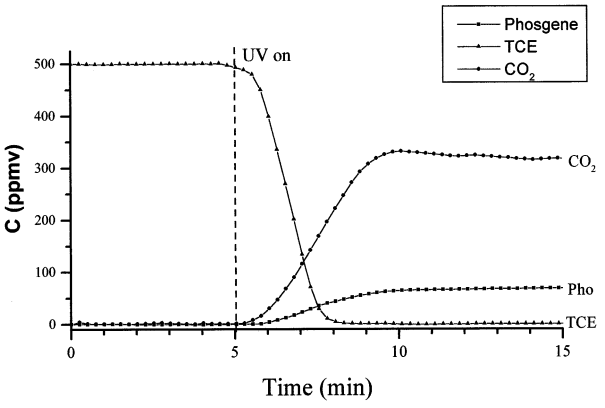

Figure 9. Diagrams of SIM-MS quantitative monitoring of TCE photocatalytic degradation normalized for instrument response to TCE, phosgene, and CO_2. Experiment was performed with 20% relative humidity and Q = 100 mL min^{-1}. Compare with the unnormalized spectrum shown in Figure 4a.

Photocatalytic Degradation Rates

Hsiao and co-workers [23] reported the following reactivity order for chloromethanes photocatalytic degradation in aqueous solution: dichloromethane > chloroform ≫ carbon tetrachloride. Ollis and co-workers [24], for chlorocarbons photocatalytic degradation in aqueous solution, reported the reactivity order: TCE > TeCE > dichloromethane > chloroform ≫ carbon tetrachloride. Under the present gas-phase TiO_2/UV photocatalytic oxidative degradation conditions, the reactivity order is: TCE ~ TeCE > dichloromethane > chloroform.

Quantitative Monitoring

Owing to different EI efficiencies of the chlorinated VOCs, the substantially different relative yields from the ionized molecules of the selected ions, and quadrupole ion transmission which varies with instrumental tuning, the intensities of the ions used for SIM-MS monitoring cannot be used for quantitative measurements.

Air mixtures containing equimolar concentrations of the starting VOC, by-products and final products can, however, be sampled in parallel (a second inlet system is available) and mass spectrometry analyzed to determine response factors for each chemical. Figures 9 exemplifies such approach by showing a SIM-MS monitoring diagram of TCE photocatalytic degradation normalized for TCE (response factor = 1.0), phosgene (4.0) and CO_2 (0.33). When using a continuous synthetic air flow of 100 mL min^{-1} and starting with 500 ppmv of TCE (compares with the corresponding unnormalized spectrum of Figure 4a), the off-gas mixture contains in the steady state mainly CO_2 (nearly 300 ppmv) and 50 ppmv of phosgene.

Conclusion

The applicability of on-line mass spectrometry and MS^2 techniques for fast and reliable monitoring and identification of by-products and final products of TiO_2/UV photocatalytic degradation of chlorinated VOCs has been demonstrated. The advantages of the system include the capability to detect, characterize, monitor, and quantify the products in real time as they are being produced and destroyed. Mass spectrometry on-line monitoring is also invaluable when rationalizing photocatalytic degradation mechanisms and determining key operation parameters for the implementation of this technology in environmental treatments.

Acknowledgment

This work was supported by the Research Support Foundation of the State of São Paulo (FAPESP) and the Brazilian National Research Council (CNPq). The authors thank Dr. K. D. Cook for invaluable discussions.

References

1. U.S. Environmental Protection Agency. Air stripping of contaminated water sources: air emissions and controls; EPA-450/3-87-017; USEPA, Washington DC, 1987.
2. Fox, M. A.; Dulay, M. T. *Chem. Rev.* **1993,** *93*, 341.
3. Hoffmann, M. R.; Martin, S. T.; Choi, W.; Bahnemann, D. W. *Chem. Rev.* **1995,** *95*, 69.
4. Pruden, A. L.; Ollis, D. F. *J. Catal.* **1983,** *82*, 404.
5. Ahmed, S.; Ollis, D. F. *Solar Energy* **1984,** *32*, 597.
6. Dibble, L. A.; Raupp, G. B. *Catal. Lett.* **1990,** *4*, 345.
7. Dibble, L. A.; Raupp, G. B. *Environ. Sci. Technol.* **1992,** *26*, 492.
8. Yamazaki-Nishida, S.; Nagano, K. J.; Phillips, L. A.; Cervera-March, S.; Anderson, M. A. *J. Photochem. Photobiol. A: Chem.* **1993,** *70*, 95.
9. Nimlos, M. R.; Jacoby, W. A.; Blake, D. M.; Milne, T. A. *Environ. Sci. Technol.* **1993,** *27*, 732.
10. Jacoby, W. A.; Nimlos, M. R.; Blake, D. M. *Environ. Sci. Technol.* **1994,** *28*, 1661.
11. Kutsuna, S.; Ebihara, Y.; Nakamura, K.; Ibusuki, T. *Atmosph. Environ.* **1993,** *27A*, 599.
12. Alberici, R. M.; Jardim, W. F. *Appl. Catal. B: Environ.* **1997,** *14*, 55.
13. (a) Juliano, V. F.; Gozzo, F. C.; Eberlin, M. N.; Kascheres, C.; Lago, C. L. *Anal. Chem.* **1996,** *68*, 1328. (b) Eberlin, M. N. *Mass Spectrom. Rev.* **1997,** *16*, 113.
14. Lu, G.; Linsebigler, A. L.; Yates, J. T., Jr. *J. Phys. Chem.* **1995**, *99*, 7626.
15. Lu, G.; Linsebigler, A. L.; Yates, J. T., Jr. *J. Chem. Phys.* **1995**, *102*, 4657.
16. Wong, J. C. S.; Linsebigler, A. L.; Lu, G.; Fan, J.; Yates, J. T., Jr. *J. Phys. Chem.* **1995,** *99*, 335.
17. Raupp, G. B.; Junio, C. T. *Appl. Surf. Sci.* **1993,** *72*, 321.
18. Kotiaho, T.; Eberlin, M. N.; Shay, B. J.; Cooks, R. G. *J. Am. Chem. Soc.* **1993,** *115*, 1004.
19. Jacoby, W. A.; Blake, D. M.; Noble, R. D.; Koval, C. A. *J. Catal.* **1995,** *157*, 87.
20. Sauer, M. L.; Hale, M. A.; Ollis, D. F. *J. Photochem. Photobiol. A: Chem.* **1995,** *88*, 169.
21. Yamazaki-Nishida, S.; Fu, X.; Anderson, M. A.; Hori, K. *J. Photochem. Photobiol. A: Chem.* **1996,** *97*, 175.
22. Lias, S. G.; Bartmess, J. E.; Liebman, J. F.; Holmes, J. L.; Levin, R. D.; Mallard, W. G. *J. Phys. Chem. Ref. Data* **1988,** *17*, Suppl. 1.
23. Hsiao, C.-Y.; Lee, C.-L.; Ollis, D. F. *J. Catal.* **1983,** *82*, 418.
24. Ollis, D. F.; Hsiao, C.-Y.; Budiman, L.; Lee, C.-L. *J. Catal.* **1984,** *88*, 89.